Journal of Applied Physics

Nonlinear optical rectification and optical bistability in a coupled asymmetric quantum dot-metal nanoparticle hybrid

Cite as: J. Appl. Phys. **124**, 113107 (2018); https://doi.org/10.1063/1.5045207
Submitted: 18 June 2018 . Accepted: 30 August 2018 . Published Online: 21 September 2018

Fernando Carreño, Miguel A. Antón, and Emmanuel Paspalakis

Nonlinear optical rectification and optical bistability in a coupled asymmetric quantum dot-metal nanoparticle hybrid

Fernando Carreño,[1] Miguel A. Antón,[1] and Emmanuel Paspalakis[2,a)]
[1]*Faculty of Optics and Optometry, University Complutense of Madrid, C/Arcos de Jalón 118, 28037 Madrid, Spain*
[2]*Materials Science Department, School of Natural Sciences, University of Patras, 265 04 Patras, Greece*

(Received 18 June 2018; accepted 30 August 2018; published online 21 September 2018)

We study the optical response of a coupled asymmetric semiconductor quantum dot-spherical metal nanoparticle structure. The asymmetric quantum dot has permanent electric dipole moments that also interact with light. We derive the density matrix equations for the system including the modification of the electric field and the exciton-plasmon coupling. We emphasize on the effects of the nonlinear optical rectification and controlled optical bistability and analyze these phenomena for different values of the light intensity and different distances between the quantum dot and the metal nanoparticle. We show that when the system is set in a situation where optical bistability can be produced, the optical rectification of the hybrid system is bivalued. We also analyze the slow-down to reach the steady state when the system is driven close and far from the turning points. *Published by AIP Publishing*. https://doi.org/10.1063/1.5045207

I. INTRODUCTION

The collective oscillations of electrons in metallic nanoparticles (MNPs) give localized surface plasmons, which lead to strong enhancement of the electromagnetic fields near the MNP. The modified electromagnetic fields cause strong interaction with quantum systems near the MNP, which in turn gives rise to strongly modified optical response of the quantum systems near the MNPs.[1,2] A prototype system to observe these effects comprises a semiconductor quantum dot (QD) and a spherical MNP. Several interesting optical effects have been studied in this hybrid nanostructure, including Fano-type phenomena in absorption of energy,[3–7] controlled coherent population transfer and ultrafast switching,[8–15] gain without inversion,[16–19] controlled optical bistability,[20–23] strongly modified resonance fluorescence,[18,24–30] and four-wave mixing,[31–34] as well as plasmon-enhanced difference-frequency generation,[35] second-harmonic generation,[36,37] terahertz emission,[38] and Kerr nonlinearity.[39] Besides on-chip nanoscale photonic nonlinear devices, the coupled QD-MNP system may also have important applications in quantum technology,[40,41] sensing,[42] and medicine.[43,44]

The purpose of the present work is to study the nonlinear optical response of an asymmetric QD coupled to a spherical MNP. Asymmetric quantum systems, such as asymmetric QDs, give rise to permanent electric dipole moments (PDMs) which also interact with light and modify significantly their optical response. Some of the phenomena that have been studied in quantum systems with PDMs include second harmonic generation[45] and high-order harmonic generation,[46] two-photon phase conjugation by degenerate four-wave mixing,[47] terahertz emission,[48,49] modifications of the saturation of absorption, dispersion, and nonlinear optical rectification,[50] and generation of correlated photon pairs,[51] as well as modified population inversion, absorption, emission, dispersion, and resonance fluorescence in bichromatically driven quantum systems with PDMs.[52–55]

In this paper, we emphasize on the phenomena of nonlinear optical rectification, which is the simplest second-order nonlinear phenomenon, and controlled optical bistability. The modification of nonlinear optical rectification has been studied in weakly probed asymmetric molecules near a periodic two-dimensional plasmonic nanostructure which significantly suppresses the spontaneous emission of the molecules leading to the enhancement of nonlinear optical rectification.[56] Here, we consider a different structure, with emphasis on the strong coupling regime, where the significant modification to the optical rectification comes from the modification of the electric field and the exciton-plasmon coupling. In addition, the phenomenon of optical bistability and its control in both steady state and transient regimes have been studied in symmetric QDs coupled to spherical MNPs.[20–23] Here, we extend these studies in asymmetric QDs coupled to spherical MNPs, including explicitly the PDMs. We present results for different values of the light intensity and the distance between the QD and the MNP. We specifically show that when the system is set in a situation where optical bistability can be produced, the nonlinear optical rectification of the hybrid system is bivalued. We also analyze the slow-down to reach the steady state when the system is driven close and far from the turning points.

For the study of the optical response of the coupled asymmetric QD-MNP hybrid, in Sec. II, we derive the relevant density matrix equations, where the effects of the PDMs are explicitly included in the equations. The presented formalism can be used for the study of several optical phenomena in the system under analysis. We then use the derived density matrix equations in Sec. III for the calculation of the nonlinear optical rectification coefficient and show the emergence of optical bistability in both steady state and transient regimes. Finally, in Sec. IV we conclude our findings.

a)Electronic mail: paspalak@upatras.gr

II. THEORETICAL MODEL

We consider an asymmetric QD with ground (excited) level $|1\rangle(|2\rangle)$, with ω_{21} being the transition frequency [see Fig. 1(a)]. We assume a transition dipole moment $\vec{\mu}_{12}$ as well as permanent dipole moments $\vec{\mu}_{11}$ and $\vec{\mu}_{22}$ which are considered to be parallel to each other and aligned along the z-axis. The system is driven by an external laser field of angular frequency (wavelength) ω (λ) and amplitude E_0 of the form

$$\vec{E}(t) = E_0 f(t)\cos(\omega t)\hat{u}_z, \tag{1}$$

where $f(t)$ is the dimensionless pulse envelope and $\hat{u}_z$ is a unitary vector along the z-axis. The dielectric constant of the QD is represented by ϵ_s. The system is located in close proximity to a spherical MNP of radius a, R being the distance between the quantum emitter and the center of the MNP [see Fig. 1(b)]. We assume that $a \ll \lambda$; thus, the interaction of the laser field with the MNP can be treated within the quasistatic approximation, $\epsilon_m(\omega)$ being the local dielectric function of the nanoparticle. Finally, we consider that both the QD and the MNP are embedded in a medium with dielectric constant ϵ_B.

The Hamiltonian of the system in the dipole approximation reads

$$\begin{aligned} H = {} & \hbar\omega_{21}|2\rangle\langle 2| - \vec{E}_{SQD}\cdot(\vec{\mu}_{11}|1\rangle\langle 1| + \vec{\mu}_{22}|2\rangle\langle 2| \\ & + \vec{\mu}_{12}|1\rangle\langle 2| + \vec{\mu}_{12}|2\rangle\langle 1|), \end{aligned} \tag{2}$$

where $\vec{E}_{SQD}$ stands for the electric field inside the QD. The density matrix obeys the equation

$$\frac{d\rho}{dt} = -\frac{i}{\hbar}[H,\rho] + \mathcal{L}\rho, \tag{3}$$

where $\mathcal{L}\rho$ describes the dissipation in the system which is introduced in a phenomenological way.

The induced polarization in the QD along the z-axis is

$$\begin{aligned} P &= N[\mu_{11}\rho_{11} + \mu_{22}\rho_{22} + \mu_{12}(\rho_{12} + \rho_{21})] - N\mu_{11} \\ &= P_1 + P_2, \end{aligned} \tag{4}$$

where

$$P_1 = \frac{N}{2}\mu(1+Z), \quad P_2 = N\mu_{12}(\rho_{12} + \rho_{21}), \tag{5}$$

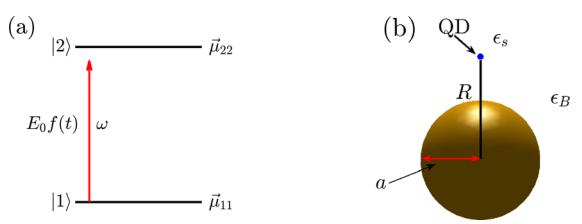

FIG. 1. (a) Energy level diagram of the two-level system with permanent electric dipole moments in the ground and excited states $\vec{\mu}_{11}$, and $\vec{\mu}_{22}$, respectively. $\vec{\mu}_{12}$ is the transition electric dipole moment. (b) The external field [$\vec{E}(t)$ as given in Eq. (1)] drives the hybrid system. The QD is considered to be a point-like emitter with dielectric constant ϵ_s, the radius of the sphere is a, and the distance of the sphere to the QD is R. The system is embedded in a medium with dielectric constant ϵ_B.

where N is the effective electron volume density in the QD system, which is defined as the ratio of the optical confinement factor and the volume of the QD,[57] and we have introduced the population difference $Z = \rho_{22} - \rho_{11}$. In addition, μ stands for $\mu = \mu_{22} - \mu_{11}$. In writing Eq. (4), we have split two terms which oscillate at very different frequencies: the term labelled as P_1 evolves in time slowly and follows the dynamics of magnitude Z. However, the term labelled as P_2 oscillates at the frequency of the laser field ω as well as other frequencies which are integer multiples of ω as we will show below.

The following step is to determine the effective electric field felt by the QD ($\vec{E}_{SQD}$) which consists of the applied, external field, $\vec{E}$, and the induced, internal field produced by the polarization of the MNP. The latter is calculated by separating out the positive and negative frequency contributions (see, for example, Refs. 4, 5, and 20) and results in

$$\vec{E}_{SQD} = \frac{\hbar}{\mu_{12}}\left(\frac{\Omega_0 f(t)}{2}e^{-i\omega t} + G\rho_{21} + cc\right)\hat{u}_z, \tag{6}$$

where Ω_0 stands for the renormalized Rabi frequency which reads[4,5]

$$\Omega_0 = \frac{\mu_{12}E_0}{\hbar\epsilon_{fs}}\left[1 + s_a\gamma_1\left(\frac{a}{R}\right)^3\right], \tag{7}$$

and the parameter G is given by[4]

$$G = \sum_{n=1}^{N_m}\frac{\mu_{12}^2}{4\pi\hbar\epsilon_B\epsilon_{fs}}(n+1)^2\frac{\gamma_n}{R^3}\left(\frac{a}{R}\right)^{2n+1}. \tag{8}$$

Here, we have used the shorthand notation $\epsilon_{fs} = (2\epsilon_B + \epsilon_s)/3\epsilon_B$, $\gamma_n = \frac{\epsilon_m(\omega)-\epsilon_B}{\epsilon_m(\omega)+(n+1)\epsilon_B/n}$, where $n = 1, 2, 3\ldots, N_m$ indicates the order of the multipole, while $s_a = 2$ since the external laser field is polarized parallel to the interparticle axis (the z-axis). Since γ_1 is a complex parameter, magnitude Ω_0 can be explicitly written in terms of its real and imaginary components, i.e., $\Omega_0 = \Omega_R + i\Omega_I$. The same holds for magnitude G, i.e., $G = G_R + iG_I$.

In view of Eq. (3), we derive the equations of motion of the density matrix elements which read

$$\begin{aligned} \hbar\frac{d}{dt}\rho_{12}(t) &= -i(-\hbar\omega_{21} + \mu E_{SQD})\rho_{12}(t) \\ &\quad + i\mu_{12}E_{SQD}Z(t) - \frac{\hbar}{T_2}\rho_{12}(t), \\ \hbar\frac{d}{dt}Z(t) &= -2i\mu_{12}E_{SQD}[\rho_{21}(t) - \rho_{12}(t)] - \frac{\hbar}{T_1}(Z(t)+1), \end{aligned} \tag{9}$$

where $T_2(T_1)$ represents the transversal(longitudinal) decay of the system.

Equation (9) contains rotating and anti-rotating terms, and now we resort to perform the rotating wave approximation (RWA). To this end, we make use of the slowly varying amplitudes defined as

$$\rho_{12}(t) = \tilde{\rho}_{12}(t)e^{\phi(t)}, \tag{10}$$

where we have made use of the shorthand notation

$$\phi(t) = i\omega t - i\frac{\mu}{\mu_{12}}\Omega_R \int_0^t f(t')\cos(\omega t')dt' - i\frac{\mu}{\mu_{12}}\Omega_I \int_0^t f(t')\sin(\omega t')dt'. \quad (11)$$

We further consider that the pulse envelope $f(t)$ is smoothly changing in time compared to ω. We also make use of the Jacobi-Auger expansion and when performing the RWA we arrive, after a series of lengthy but straightforward calculations, at the following equations for the optical coherence and the population difference

$$\begin{aligned}\frac{d}{dt}\tilde{\rho}_{12}(t) = &-\left(\frac{1}{T_2}+i\delta\right)\tilde{\rho}_{12}(t) + iG^*\tilde{\rho}_{12}(t)Z(t) \\ &+i\frac{\Omega_0^*}{2}f(t)Z(t)\hat{A} + i\frac{\Omega_0}{2}f(t)Z(t)\hat{B} \\ &+iG\tilde{\rho}_{21}(t)Z(t)\hat{C} - i\frac{\mu G}{\mu_{12}}\tilde{\rho}_{21}(t)\tilde{\rho}_{12}(t)\hat{D} \\ &-i\frac{\mu G^*}{\mu_{12}}\tilde{\rho}_{12}^2(t)\hat{D}^*, \end{aligned} \quad (12)$$

$$\begin{aligned}\frac{d}{dt}Z(t) = &-\frac{1}{T_1}[1+Z(t)] - 4G_I\tilde{\rho}_{21}(t)\tilde{\rho}_{12}(t) \\ &-i\Omega_R f(t)\tilde{\rho}_{21}(t)\left(\hat{A}+\hat{B}\right) + i\Omega_R f(t)\tilde{\rho}_{12}(t)\left(\hat{A}^*+\hat{B}^*\right) \\ &-\Omega_I f(t)\tilde{\rho}_{21}(t)\left(\hat{A}-\hat{B}\right) - \Omega_I f(t)\tilde{\rho}_{12}(t)\left(\hat{A}^*-\hat{B}^*\right) \\ &-2iG\tilde{\rho}_{21}^2(t)\hat{C} + 2iG^*\tilde{\rho}_{12}^2(t)\hat{C}^*. \end{aligned}$$

In writing Eq. (12), we have introduced the detuning $\delta = \omega - \omega_{21}$, and the following abbreviations:

$$\begin{aligned}\hat{A} &= \sum_{k=-\infty}^{+\infty}(-i)^k J_k(\alpha_R)J_k(\alpha_I), \\ \hat{B} &= \sum_{k=-\infty}^{+\infty}(-i)^k J_{k+2}(\alpha_R)J_k(\alpha_I), \\ \hat{C} &= \sum_{k=-\infty}^{+\infty}(-i)^k J_{k+2}(2\alpha_R)J_k(2\alpha_I), \\ \hat{D} &= \sum_{k=-\infty}^{+\infty}(-i)^k J_{k+1}(\alpha_R)J_k(\alpha_I), \end{aligned} \quad (13)$$

where $\alpha_R = \frac{\mu}{\omega\mu_{12}}\Omega_R f(t)$, and $\alpha_I = \frac{\mu}{\omega\mu_{12}}\Omega_I f(t)$. Note that magnitudes in Eq. (13) involve the coupling of Bessel functions of the same order for $\hat{A}$, whereas for magnitude $\hat{D}$ the coupling involves Bessel functions of adjacent orders. Also, in the case of magnitudes $\hat{B}$ and $\hat{C}$ the coupling involve Bessel functions whose orders differ by two. In view of that and taking into account the properties of the Bessel functions, we expect that the importance of these parameters in descending order should be $\hat{A}$, $\hat{D}$, $\hat{C}$, and $\hat{B}$. It is worth noting that in view of Eq. (12) we recover the result for the non-polar system in the case that $\mu = 0$, which in turn results in $\hat{A} = 1.0$, and $\hat{B} = \hat{C} = \hat{D} = 0$. The existence of PDMs introduces new couplings in the time evolution of the population difference and the optical coherence. A close look at the equation of motion for the population difference reveals the appearance of nonlinear couplings involving G and the parameters introduced in Eq. (13).

The nonlinear optical rectification coefficient accounts for the DC component of the induced polarization of the QD given in Eq. (4). This DC component (P_{dc}) has two contributions: one arises from the term P_1 as defined in Eq. (5), and the second term arises from the DC component of P_2. The two mentioned contributions must be evaluated at steady state. By taking into account the fact that $P_{dc} = \epsilon_0\chi_0 E_0^2/4$, and by isolating the non-oscillating terms in P_2, we arrive at the following identity:

$$\epsilon_0\chi_0 E_0^2/4 = N\mu_{12}\left[\tilde{\rho}_{12}(\infty)\hat{D}^* + \tilde{\rho}_{21}(\infty)\hat{\mu}\right] + \frac{N}{2}\mu[1+Z(\infty)], \quad (14)$$

which allows one to derive the nonlinear optical rectification coefficient χ_0 by solving Eq. (12).

III. NUMERICAL RESULTS

We consider a QD with a semi-parabolic confining potential with angular frequency $\bar{\omega}$, a model that has been used in several studies, see for example Refs. 58–61. Within the semi-parabolic confining potential model, for specific QD materials, the induced and the permanent electric dipole moments as well as the transition energy are determined solely by the angular frequency $\bar{\omega}$. Choosing the transition frequency $\hbar\omega_{21} = 2\hbar\bar{\omega} = 2.4\,\text{eV}$, we obtain for CdSe-type QDs the transition dipole moment as $\mu_{12} = 0.365\ e$ nm, and the difference of the PDMs as $\mu = 0.447\ e$ nm, respectively. The permittivity of the QD is $\epsilon_s = 6\epsilon_0$, embedded in vacuum ($\epsilon_B = \epsilon_0$). The relaxation times considered are $T_1 = 0.8\,\text{ns}$ and $T_2 = 0.3\,\text{ns}$. The electron density is taken as $N = 5\times10^{20}\ \text{m}^{-3}$. As for the MNP, we consider a gold sphere with a radius of $a = 10\,\text{nm}$, whereas the values for $\epsilon_m(\omega)$ are obtained through interpolation of the experimental values for gold.[62] Note that the relaxation times T_1 and T_2 are also influenced by the presence of the MNP but in the present case and in the frequency range considered, the values of T_1 and T_2 can be taken as constant, as in previous works in similar systems.[3–26,28,31–39] In what follows, we set $\Gamma_0 = 1/T_2$; thus, the different parameters (Rabi frequency, detuning, etc.) in Eq. (12) can be rewritten in normalized units.

A. Steady state results: Nonlinear optical rectification and optical bistability

As a first step in our study, we evaluate the relevance of the new terms defined in Eq. (13). We compute the modulus of those coefficients as a function of the distance R, and the results are presented in Fig. 2, when the laser field is tuned to resonance with the optical transition ($\delta = 0$) and its intensity is set to $I = 10^6\ \text{W/m}^2$, which roughly corresponds to a free space Rabi frequency of $1.7\Gamma_0$. The $\hat{A}$ parameter is the largest one, and its deviations from unity (which represents the

situation of a quantum emitter without PDMs) are very small (solid line). The following relevant parameter is $\hat{D}$, and it has been scaled by 10^{-5} to fit in the same vertical scale as $1-|\hat{A}|$. The other two parameters $\hat{C}$ (dashed-dotted line) and $\hat{B}$ (dashed line) are the ones which take the smallest values. It should be noted that the vertical scale in Fig. 2 should be modified when the intensity of the laser field is changed but the same trend will remain for the spatial variation of the coefficients listed in Eq. (13). The numerical results obtained confirm the qualitative analysis presented after Eq. (13).

In what follows, we assume that the hybrid system is under constant illumination ($f(t)=1$). We further consider that initially the QD is in the ground state with null initial coherence ($Z(0)=-1$, $\tilde{\rho}_{12}(0)=0$). The coupled set of Eq. (12) is solved using an adaptive fourth-fifth order Runge-Kutta algorithm. The effect of multipoles of the MNP is taken into account to determine the parameter G by setting the number $N_m=10$, as we found this to provide converging results. We have selected different values of the intensity of the driving field (I), and we have determined the steady state values of the population difference and the optical coherence for several values of the optical detuning δ, which in turn allows us to determine $\chi_0(\delta)$ as given in Eq. (14). We note that the main contribution in $\chi_0(\delta)$ comes from the second term on the right hand side of Eq. (14). The first term on the right hand side of Eq. (14) provides a small contribution to $\chi_0(\delta)$.

The nonlinear optical rectification is displayed in Figs. 3(a)–3(c) for three different values of the intensity of the laser field and several distances between the QD and the MNP. As for the lowest intensity shown in Fig. 3(a), we can devise that there is a redshift of the peak at which the optical rectification is maximum as the MNP approaches the QD. The shift is accompanied with a broadening of the curves and a decrease in the peak maximum. In addition, the curves increase their asymmetry around the peak maximum as the MNP is set closer to the QD. Figure 3(b) shows the curves obtained when the laser intensity is increased up to 5×10^6 W/m^2 and shows a similar qualitative behaviour as before except for the following: (i) the redshift is better appreciated for the shortest distance; (ii) the broadening of the curves is larger; and (iii) the asymmetry is stronger than in the previous case. In view of these results, we recover for $\chi_0(\delta)$ a similar behaviour as the one previously found for the upper state population in Ref. 9 except for the fact that in our work we make use of a larger value of the laser field intensity which in turn is responsible for the emergence of the asymmetries found.

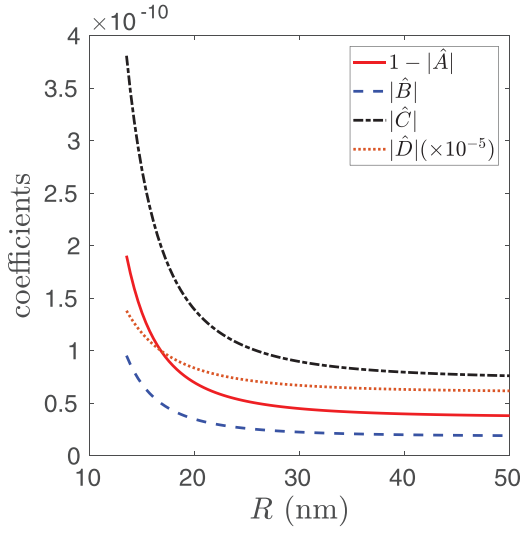

FIG. 2. Modulus of the coefficients defined in Eq. (13) as a function of the distance R between the QD and the MNP. The laser field is resonant with the QD transition ($\delta=0$) and its intensity is set to $I=10^6$ W/m^2.

Finally in Fig. 3(c), we show the results obtained for the largest intensity. Here, the most striking result relies in the fact that for the shortest distance the nonlinear optical rectification coefficient exhibits a sudden drop. Such an abrupt change obtained for the shortest distance is an indication that we are driving the system through the region where optical bistability is obtained. Thus, the numerical procedure used to determine the optical rectification fails to give the full physical picture, and we resort to obtain it through an approximate method. We want to remind that the problem of optical bistability in a non-polar hybrid system has been extensively analyzed by Malyshev *et al.*[20–22] Here, we resort to obtain an analytical approximation of the optical bistability of the current (polar) hybrid system by neglecting the coefficients $\hat{B}$, $\hat{C}$ and $\hat{D}$, while keeping $\hat{A}$ in Eq. (12). This approximation is justified since the most important coefficient is $\hat{A}$ as we have shown after the discussion following Fig. 2. Under such conditions, the steady-state population difference ($Z=Z(\infty)$) can be shown to obey the following third order polynomial:

$$aZ^3+bZ^2+cZ+d=0, \tag{15}$$

where the coefficients appearing in Eq. (15) are given by

$$\begin{aligned} a&=\Gamma_0|G|^2,\\ b&=\Gamma_0|G|^2-2\Gamma_0(\gamma G_I+\delta G_R),\\ c&=\Gamma_0(\gamma^2+\delta^2)-2\Gamma_0(\gamma G_I+\delta G_R)+\gamma|\hat{A}|^2|\Omega_0|^2,\\ d&=\Gamma_0(\gamma^2+\delta^2). \end{aligned} \tag{16}$$

Equation (15) can be solved using a root finding algorithm, and by keeping the real roots we obtain the approximate curves of optical bistability. Once we determine the different values of Z, we derive the corresponding steady-state values for the optical coherence. The solutions found for the case with $R=15$ nm, and $\delta=-20\Gamma_0$ versus the intensity of the laser field (I) are displayed in Fig. 4(a). There we can see that when the intensity I is in the interval determined by the turning points ($[I_i, I_s]$), three real roots are obtained, the lower and upper branches being the so called "stable" solutions. The intensity used to produce Fig. 3(c) belongs to this interval; thus, when solving Eq. (12) for a constant driving field, we only reach one of the multiple solutions. This is the origin of the sudden fall of the optical rectification coefficient displayed in the solid curve in Fig. 3(c). In other words, when we reach a region of the parameter space of the system where optical bistability is obtained, we should evaluate the optical rectification coefficient for the multiple stable

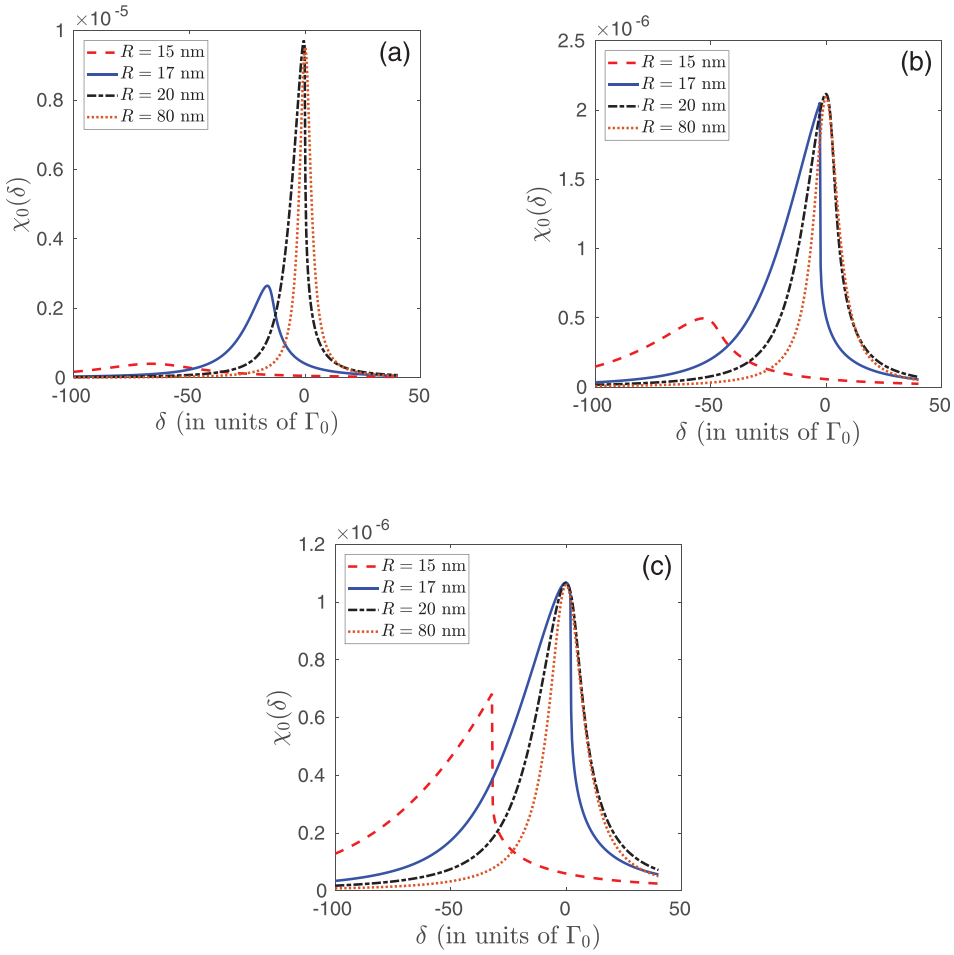

FIG. 3. Nonlinear optical rectification $\chi_0(\delta)$ in m/V versus the optical detuning δ for several distances of the QD to the MNP: $R = 15$ nm (dashed curve), $R = 17$ nm (solid curve), $R = 20$ nm (dashed-dotted curve), and $R = 80$ nm (dotted curve) for (a) $I = 10^6$ W/m^2, (b) $I = 5 \times 10^6$ W/m^2, and (c) $I = 10^7$ W/m^2.

solutions available. This is done for the case with $R = 15$ nm and $I = 10 \times 10^6$ W/m^2 while varying the detuning, and the results are displayed in Fig. 4(b), where two vertical thin dotted lines have been drawn to indicate the region where bistability is produced.

B. Transient results: Critical and non-critical slow-down

In the previous analysis, we have focused on the steady-state behaviour of the hybrid system. Here, we turn our attention on the influence of PDMs on the time dynamics of the system close to the turning point I_s. This problem has been previously addressed in several works where the relaxation time of the population difference has been analyzed for non-polar hybrid systems.[8,21] Also, this behaviour has been previously described in bistable systems (see, for example, Ref. 63). In the current system, if we tune the intensity of laser field (I) around I_s, it has been shown that the steady-state is reached after a switching time which depends on the closeness of I to I_s. For the parameters used to produce Fig. 4(a), the value of I_s is determined numerically to be given by $I_s = 17.286 \times 10^6$ W/m^2. We solve the time evolution in Eq. (12) when the intensity is set to $I = 17.304 \times 10^6$ W/m^2, and the results are displayed in Fig. 5(a) for the non-polar (polar) hybrid system with a solid (dashed) curve. Here, we can

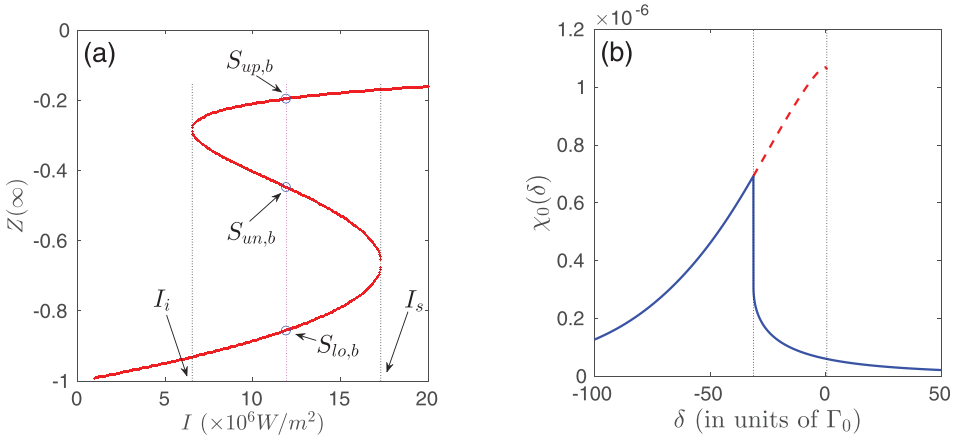

FIG. 4. (a) Steady state population difference $[Z = Z(\infty)]$ versus the intensity of the incident optical field I for the case with $R = 15$ nm, and $\delta = -20\Gamma_0$. (b) Nonlinear optical rectification $\chi_0(\delta)$ in m/V versus the optical detuning δ for the case with $R = 15$ nm, and $I = 10^7$ W/m^2. The two vertical thin dotted curves determine the region where optical bistability is obtained.

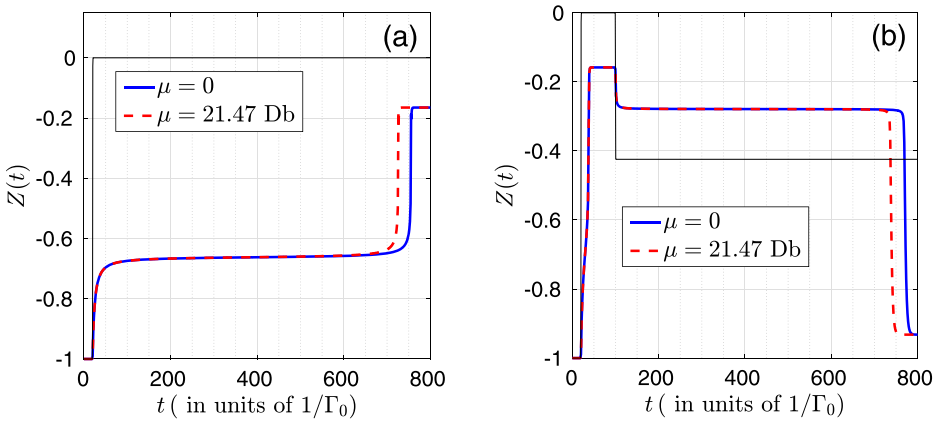

FIG. 5. Time evolution of population difference for the case where the laser field intensity is set to (a) $I = 17.304 \times 10^6$ W/m^2, and (b) $I = 20 \times 10^6$ W/m^2. The rest of parameters are $R = 15$ nm and $\delta = -20\Gamma_0$. Solid (dashed) curve stands for the non-polar (polar) hybrid system. The thin dashed-dotted curve in panel (b) displays the temporal profile $f_0(t)$ as defined in Eq. (17) for the case with $v_f = 0.214513$, $t_0 = 20$, $t_p = 100$, $p_r = p_f = 5$.

devise that although the final value of population difference is nearly the same (their difference being on the order of 10^{-7}), the switching time slightly differs: the effect of the non-linear terms arising from the coupling with PDMs in Eq. (12) is to shorten the switching time. The closeness of the steady-state population difference achieved for the polar and non-polar hybrid system allows one to justify the approximations made to reach Eq. (15).

The critical slow-down (or metaresonance as introduced in Ref. 8) found when we drive the system close to I_s can also be obtained if we set the system close to I_i. In this case, I_i is found numerically to be given by $I_i = 6.540 \times 10^6$ W/m^2. To this end, we set the initial intensity $I > I_s$ during a certain time interval such that after the initial transient the system reaches the steady state in the upper branch of Fig. 4(a). Then we allow for a decrease in the intensity until the point I_s is reached. Let the amplitude profile driving the system to vary according to $f(t) = f_0(t)$, where $f_0(t)$ is the slowly varying in time pulse envelope which reads as

$$f_0(t) = 0.5 - v_f + 0.5 \times \tanh[p_r(t - t_0)] - v_f \times \tanh\left[p_f(t - t_p)\right], \quad (17)$$

where t_0 (t_p) stands for the switching on (off) of the laser field, and p_r (p_f) indicates the inverse of the rising (falling) time. Finally, v_f is a parameter which allows one to select the final value of the intensity. The results of the numerical simulations carried out are shown in Fig. 5(b) for the non-polar (polar) hybrid system with a solid (dashed) curve. The thin dashed curve indicates the time evolution of $f_0(t)$ given in Eq. (17). Note that when the system is driven under this way, we also observe the critical slow-down which, for the polar case (dashed curve), manifests in a shortening of the switching time with respect to the non-polar case (solid curve). This could be of interest for the design of ultracompact optical delay lines. Moreover, since the slow-down is very sensitive to the closeness of the driving intensity to I_s, the current system may be useful in the design of electric field to time converters.

In addition to the critical slow-down, it is well known from the early works in optical bistability that such large values for the switching time can be also obtained when such a system is driven far from the turning points of the domain of bistability (see, for example, Refs. 64–66). Here we show that the current hybrid system can exhibit such behaviour. To this end, let us consider that the system is driven at an intensity I_m which is located at the center of the interval [I_i, I_s] [see Fig. 4(a)]. Note that for this value of the intensity there are three possible values for the population difference: one in the lower branch ($S_{lo,b}$), one in the upper branch ($S_{up,b}$), and one in the intermediate unstable branch ($S_{un,b}$). Let us assume that the system is prepared in the lower state ($S_{lo,b}$). After that, we apply a rectangular pulse with intensity $I_m + I_1$ during a certain time interval t_p which drives the system far from the point I_s. Under such conditions, we can set the system to the upper state ($S_{up,b}$). We will show that with a proper choice of the product $I_1 t_p$, we can bring the system either back to the lower state or to the upper state. It is intuitive that there will exist a critical value for t_p that will set the

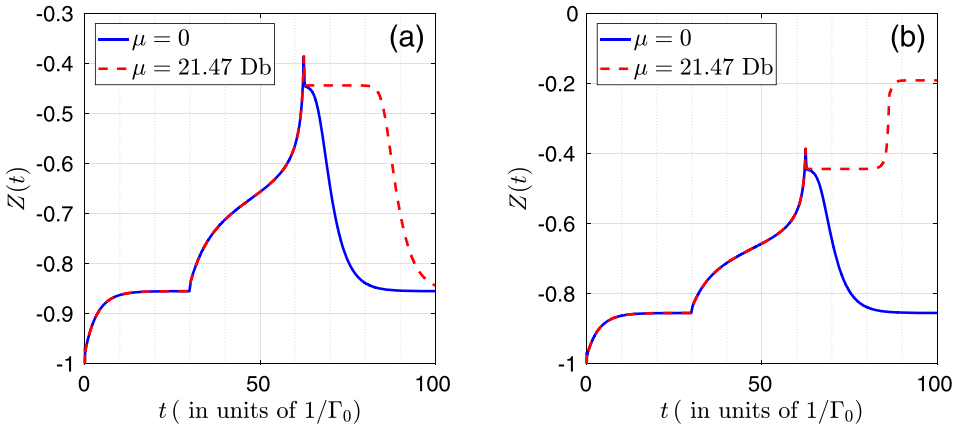

FIG. 6. Time evolution of population difference for the case where the laser field intensity is set to $I_m = 11.912 \times 10^6$ W/m^2, $I_1 = (6.643 \times 10^5 + \epsilon)$ W/m^2 (a) $\epsilon > 0$, and (b) $\epsilon < 0$. The rest of parameters are $R = 15$ nm and $\delta = -20\Gamma_0$. Solid (dashed) curve stands for the non-polar (polar) hybrid system. The thin solid curves display the temporal profile $f_0(t)$ as defined in Eq. (18) for the case with $t_0 = 30$, $t_p = 2.5$.

system in the unstable middle state ($S_{un,b}$). The time varying intensity applied to the hybrid system is given by

$$I(t) = \begin{cases} I_m & t < t_0 \\ I_m + I_1 & t <= t_0 <= (t_0 + t_p) \\ I_m & t > (t_0 + t_p). \end{cases} \quad (18)$$

The results of the numerical simulations are shown in Fig. 6, where the values of ϵ used to produce the panels were finely tuned around I_1. Here, we observe that the system can be set either to the lower or upper states, while before reaching the steady state, the population difference remains in an intermediate state even after switching I_t to the initial value I_m. The period of time where the system remains in the intermediate state can be finely tuned by varying ϵ. Here we want to stress that the driving to the intermediate state has been optimized for the polar case although this behaviour could also be obtained for the non-polar hybrid system by appropriate tuning of the driving intensities.

IV. CONCLUSIONS

In this work, we analyze the optical response of a hybrid system comprised of an asymmetric QD and a metallic nanosphere coupled to each other through the dipole-dipole interaction. The QD is modelled as a two-level system with PDMs. We have derived the density matrix equations which describe the time evolution of the optical coherence and the population difference where new nonlinear terms emerge as a consequence of the dipole-dipole interaction with the MNP. This formalism can be used for the study of various optical effects of coupled asymmetric QD-MNP hybrids. Here, we present numerical results which show how the nonlinear optical rectification is modified due to the exciton-plasmon coupling. We show that when the system is driven under constant illumination in a situation where optical bistability can be produced, the optical rectification of the hybrid system is bivalued. Here the main effect of PDMs is to allow for the existence of optical rectification since their effect on the effective field experienced by the QD is reduced. This can be understood by taking a close look at the argument of the Bessel functions appearing in Eq. (13) which involve α_R and α_I (except for $\hat{C}$ whose argument is twice those values). In view of that, the importance of the new couplings (magnitudes $\hat{D}$, $\hat{C}$, and $\hat{B}$) will be relevant in cases where the overlap between the Bessel functions takes large values, which in turn requires $|\alpha_R| \gg 1$, and $|\alpha_I| \gg 1$. This could be achieved (i) by designing a quantum emitter with large values of $\frac{\mu}{\mu_{12}}$; (ii) by moving to a range of frequencies where the quotient $\frac{\Omega_R}{\omega}$ is not so small as the one obtained when ω lies in the optical range; and (iii) by a combination of the previous two.

We have also analyzed the time dynamics of the hybrid system, and we have found that when the system is driven close to the turning points, the slow-down to reach the steady state depends on the presence of PDMs and results in the shortening of the switching time compared to the non-polar case. We have also found that the system can be driven to the unstable state for a controlled period of time by fine tuning of the driving intensity. By a proper tuning of the driving intensity, the system can be set either to the upper state or back to the lower state of the bistability curve. The simulations carried out indicate that the current nanoscale hybrid system supports many of the features found in bistable devices[63,64] and may allow for the development of ultracompact optical delay lines, electric field to time converters, and electrometers.

ACKNOWLEDGMENTS

M.A.A. and F.C. acknowledge the support of UCM-Banco de Santander Research Project PR41/17-21033 and the support of MICINN through Project FIS2017-87360-P.

[1]M. S. Tame, K. R. McEnery, S. K. Özdemir, J. Lee, S. A. Maier, and M. S. Kim, Nat. Phys. **9**, 329 (2013).
[2]P. Vasa and C. Lienau, ACS Photonics **5**, 2 (2018).
[3]W. Zhang, A. O. Govorov, and G. W. Bryant, Phys. Rev. Lett. **97**, 146804 (2006).
[4]J.-Y. Yan, W. Zhang, S.-Q. Duan, X.-G. Zhao, and A. O. Govorov, Phys. Rev. B **77**, 165301 (2008).
[5]R. D. Artuso and G. W. Bryant, Phys. Rev. B **82**, 195419 (2010).
[6]M. R. Singh, D. G. Schindel, and A. Hatef, Appl. Phys. Lett. **99**, 181106 (2011).
[7]S. G. Kosionis, A. F. Terzis, V. Yannopapas, and E. Paspalakis, J. Phys. Chem. C **116**, 23663 (2012).
[8]S. M. Sadeghi, Phys. Rev. B **79**, 233309 (2009).
[9]S. M. Sadeghi, Nanotechnology **20**, 225401 (2009).
[10]M. A. Antón, F. Carreño, S. Melle, O. G. Calderón, E. Cabrera-Granado, J. Cox, and M. R. Singh, Phys. Rev. B **86**, 155305 (2012).
[11]A. Hatef, S. M. Sadeghi, and M. R. Singh, Nanotechnology **23**, 205203 (2012).
[12]M. A. Antón, F. Carreño, S. Melle, O. G. Calderón, E. Cabrera-Granado, and M. R. Singh, Phys. Rev. B **87**, 195303 (2013).
[13]E. Paspalakis, S. Evangelou, and A. F. Terzis, Phys. Rev. B **87**, 235302 (2013).
[14]W.-X. Yang, A.-X. Chen, Z. Huang, and R.-K. Lee, Opt. Express **23**, 13032 (2015).
[15]R. J. McMillan, L. Stella, and M. Grüning, Phys. Rev. B **94**, 125312 (2016).
[16]S. M. Sadeghi, Nanotechnology **21**, 455401 (2010).
[17]S. G. Kosionis, A. F. Terzis, S. M. Sadeghi, and E. Paspalakis, J. Phys.: Condens. Matter **25**, 045304 (2013).
[18]S. M. Sadeghi, Phys. Rev. A **88**, 013831 (2013).
[19]D.-X. Zhao, Y. Gu, J. Wu, J.-X. Zhang, T.-C. Zhang, B. D. Gerardot, and Q.-H. Gong, Phys. Rev. B **89**, 245433 (2014).
[20]A. V. Malyshev and V. A. Malyshev, Phys. Rev. B **84**, 035314 (2011).
[21]B. S. Nugroho, A. A. Iskandar, V. A. Malyshev, and J. Knoester, J. Chem. Phys. **139**, 014303 (2013).
[22]B. S. Nugroho, V. A. Malyshev, and J. Knoester, Phys. Rev. B **92**, 165432 (2015).
[23]A. Mohammadzadeh and M. Miri, J. Appl. Phys. **123**, 043111 (2018).
[24]A. Ridolfo, O. Di Stefano, N. Fina, R. Saija, and S. Savasta, Phys. Rev. Lett. **105**, 263601 (2010).
[25]E. Waks and D. Sridharan, Phys. Rev. A **82**, 043845 (2010).
[26]S. M. Sadeghi, Appl. Phys. Lett. **101**, 213102 (2012).
[27]R. C. Ge, C. Van Vlack, P. Yao, J. F. Young, and S. Hughes, Phys. Rev. B **87**, 205425 (2013).
[28]F. Carreño, M. A. Antón, and F. Arrieta-Yáñez, Phys. Rev. B **88**, 195303 (2013).
[29]M. A. Antón, F. Carreño, O. G. Calderón, S. Melle, and E. Cabrera, J. Opt. **18**, 025001 (2016).
[30]F. Carreño, M. A. Antón, V. Yannopapas, and E. Paspalakis, Phys. Rev. A **94**, 013834 (2016).
[31]J.-B. Li, N.-C. Kim, M.-T. Cheng, L. Zhou, Z.-H. Hao, and Q.-Q. Wang, Opt. Express **20**, 1856 (2012).
[32]E. Paspalakis, S. Evangelou, S. G. Kosionis, and A. F. Terzis, J. Appl. Phys. **115**, 083106 (2014).
[33]J.-J. Li and K.-D. Zhu, Crit. Rev. Solid State Mater. Sci. **39**, 25 (2014).
[34]S. K. Singh, M. K. Abak, and M. E. Tasgin, Phys. Rev. B **93**, 035410 (2016).

[35]J.-Y. Yan, W. Zhang, S.-Q. Duan, and X.-G. Zhao, J. Appl. Phys. **103**, 104314 (2008).
[36]M. R. Singh, Nanotechnology **24**, 125701 (2013).
[37]D. Turkpence, G. B. Akguc, A. Bek, and M. E. Tasgin, J. Opt. **16**, 105009 (2014).
[38]F. Carreño, M. A. Antón, S. Melle, O. G. Calderón, E. Cabrera-Granado, J. Cox, M. R. Singh, and A. Egatz-Gómez, J. Appl. Phys. **115**, 064304 (2014).
[39]A. F. Terzis, S. G. Kosionis, J. Boviatsis, and E. Paspalakis, J. Mod. Opt. **63**, 451 (2016).
[40]J. Hakami and M. S. Zubairy, Phys. Rev. A **93**, 022320 (2016).
[41]N. Iliopoulos, I. Thanopulos, V. Yannopapas, and E. Paspalakis, Phys. Rev. B **97**, 115402 (2018).
[42]S. M. Sadeghi, C. Mao, S. M. Sadeghi, and C. Mao, J. Appl. Phys. **121**, 014309 (2017).
[43]M. R. Singh, J. Guo, J. M. J. Cid, J. E. De, and H. Martinez, J. Appl. Phys. **121**, 094303 (2017).
[44]M. R. Singh, M. C. Sekhar, S. Balakrishnan, and S. Masood, J. Appl. Phys. **122**, 034306 (2017).
[45]R. Bavli and Y. B. Band, Phys. Rev. A **43**, 507 (1991).
[46]O. G. Calderón, R. Gutierrez-Castrejon, and J. M. Guerra, IEEE J. Quantum Electron. **35**, 47 (1999).
[47]M. A. Antón and I. Gonzalo, J. Opt. Soc. Am. B **8**, 1035 (1991).
[48]O. V. Kibis, G. Y. Slepyan, S. A. Maksimenko, and A. Hoffmann, Phys. Rev. Lett. **102**, 023601 (2009).
[49]K. V. Kavokin, M. A. Kaliteevski, R. A. Abram, A. V. Kavokin, S. Sharkova, and I. A. Shelykh, Appl. Phys. Lett. **97**, 201111 (2010).
[50]E. Paspalakis, J. Boviatsis, and S. Baskoutas, J. Appl. Phys. **114**, 153107 (2013).
[51]F. Oster, C. H. Keitel, and M. Macovei, Phys. Rev. A **85**, 063814 (2012).
[52]M. Macovei, M. Mishra, and C. H. Keitel, Phys. Rev. A **92**, 013846 (2015).
[53]Y. Yan, Z. Lü, H. Zheng, and Y. Zhao, Phys. Rev. A **93**, 033812 (2016).
[54]G. Y. Kryuchkyan, V. Shahnazaryan, O. V. Kibis, and I. A. Shelykh, Phys. Rev. A **95**, 013834 (2017).
[55]M. A. Antón, S. Maede-Razavi, F. Carreño, I. Thanopulos, and E. Paspalakis, Phys. Rev. A **96**, 063812 (2017).
[56]I. Thanopulos, E. Paspalakis, and V. Yannopapas, Phys. Rev. B **85**, 035111 (2012).
[57]C.-J. Chang-Hasnain, P.-C. Ku, J. Kim, and S.-L. Chuang, Proc. IEEE **91**, 1884 (2003).
[58]Y.-B. Yu, S.-N. Zhu, and K.-X. Guo, Phys. Lett. A **335**, 175 (2005).
[59]S. Baskoutas, E. Paspalakis, and A. F. Terzis, Phys. Rev. B **74**, 153306 (2006).
[60]I. Karabulut, H. Safak, and M. Tomak, J. Phys. D: Appl. Phys. **41**, 155104 (2008).
[61]J. E. Q. Bautista, M. L. Lyra, and R. P. A. Lima, Opt. Express **22**, 28270 (2014).
[62]P. B. Johnson and R. W. Christy, Phys. Rev. B **6**, 4370 (1972).
[63]R. Bonifacio and P. Meystre, Opt. Commun. **29**, 131 (1979).
[64]J. Y. Bigot, A. Daunois, and P. Mandel, Phys. Lett. A **123**, 123 (1987).
[65]B. Segard, J. Zemmouri, and B. Macke, Opt. Commun. **63**, 339 (1987).
[66]F. Mitschke, C. Boden, W. Lange, and P. Mandel, Opt. Commun. **71**, 385 (1989).